# Controlling high-harmonic generation and above-threshold ionization with an attosecond-pulse train

C. Figueira de Morisson Faria[1], P. Salières[2], P. Villain[2], and M. Lewenstein[3,4]
[1] *Centre for Mathematical Science, City University, Northampton Square, London EC1V 0HB, United Kingdom*
[2] *CEA-SPAM, Bât. 522, Centre d'Etudes de Saclay, F-91191 Gif-Sur-Yvette, France*
[3] *ICREA, Institució Catalana di Recerca i Estudis Avançats, and ICFO, Institut de Ciències Fotòniques, E-08860 Castelldefels (Barcelona), Spain*
[4] *Institut für theoretische Physik, Universität Hannover, Appelstr. 2, D-30167 Hannover, Germany*
(Dated: June 12, 2006)

We perform a detailed analysis of how high-order harmonic generation (HHG) and above-threshold ionization (ATI) can be controlled by a time-delayed attosecond-pulse train superposed to a strong, near-infrared laser field. In particular we show that the high-harmonic and photoelectron intensities, the high-harmonic plateau structure and cutoff energies, and the ATI angular distributions can be manipulated by changing this delay. This is a direct consequence of the fact that the attosecond pulse train can be employed as a tool for constraining the instant an electronic wave packet is ejected in the continuum. A change in such initial conditions strongly affects its subsequent motion in the laser field, and thus HHG and ATI. In our studies, we employ the Strong-Field Approximation and explain the features observed in terms of interference effects between various electron quantum orbits. Our results are in agreement with recent experimental findings and theoretical studies employing purely numerical methods.



## I. INTRODUCTION

High-frequency light pulses of attosecond ($10^{-18}s$) duration have caused a breakthrough in metrology, allowing one to resolve and control dynamical processes occurring in the subfemtosecond and subangström scale [1]. This is in particular possible due to the fact that one attosecond is roughly the time it takes for light to travel through atomic distances. Attosecond pulses may be used, for instance, for tracing the motion of bound electrons [2], exciting inner shell electrons [3], controlling molecular motion [4], electron emission [5], high-harmonic generation [6, 7] or above-threshold ionization [8].

Such pulses owe their existence to the fact that high-order harmonics, which are generated by rare gases interacting with intense ($I \sim 10^{14}\mathrm{W/cm^2}$), near-infrared (IR) laser fields of femtosecond duration, are nearly phase locked. Hence, by superposing a large number of harmonics one may obtain attosecond pulses in the extreme ultraviolet range [1]. There exist two approaches to attosecond-pulse production. One may generate isolated attosecond pulses from few-cycle laser pulses [2, 9, 10], or attosecond-pulse trains from laser pulses comprising several cycles [11]. Such attosecond pulse trains have been predicted in the late 1990's [12], and experimentally realized a few years later [11]. Since then, there has been considerable improvement in their contrast, duration and peak intensity. In particular, an intrinsic chirp of the attosecond emission was evidenced, setting a lower limit on the duration of the attosecond pulses obtained by grouping an increasing number of harmonic orders [13]. Thereby, important issues are an adequate choice of the group of harmonics, and optimal propagation conditions in the gaseous media. In this context, it is of interest to control the atto-chirp and more generally the intensity- and order-dependent phase of the atomic dipole [14].

Recently, it has been shown that an attosecond-pulse train superposed to an intense laser field can be used for manipulating high-order harmonic generation (HHG) [6, 7] and above-threshold ionization (ATI) [8]. In particular, the resolution, intensity and maximal energies of both ATI and HHG spectra turned out to be strongly dependent on the time delay between the laser field and the attosecond pulse train. This behavior has been predicted theoretically [6, 8] and observed experimentally in both cases [7, 8]. It has been interpreted in the light of the physical mechanisms governing both phenomena.

In HHG, an electron reaches the continuum by tunneling or multiphoton ionization at a time $t'$, propagates in the continuum and, subsequently, at a time $t$, recombines with its parent ion [15]. In this process, the kinetic energy acquired by this electron is released in form of high-frequency radiation. Similarly, for ATI, an electron leaves an atom, either reaching the detector, or elastically recolliding with it. This leads to the low- or high-order ATI peaks, respectively. The attosecond pulse train can be used for controlling the ejection of such an electron in the continuum. Specifically, the time $t'$ can be fixed by changing the time delay between the attosecond pulse train and the IR field. This constraint upon the ionization time can be used as a tool for selecting a particular orbit of an electron reaching the continuum [6, 7], or a particular momentum transfer from the IR field to the electron [8]. As a direct consequence, the ATI and HHG spectra can be manipulated.

In this paper, we investigate the effects reported in [6, 7, 8] for HHG and ATI in detail, using a quantum-mechanical formulation of the above-stated processes [16, 17, 18], within the Strong-Field Approximation (SFA) [19]. This approach has some advantages over

that employed in [6, 8], i.e., the numerical solution of the time-dependent Schrödinger equation (TDSE). Indeed, even though the SFA involves a higher degree of modeling and physical approximations, it is much less demanding, from the computational viewpoint. This is particularly important for a realistic description of the macroscopic response of the gaseous system, in which the single-atom response serves as input for propagation codes. Furthermore, it provides a transparent and clear physical interpretation, in terms of the orbits of an electron leaving or recombining with its parent ion. This is a further advantage over the TDSE, for which it may be difficult to extract the physical mechanisms involved.

In this work, we put a particularly strong emphasis on the quantum interference between the different possible paths of an electron ejected by the attosecond-pulse train. Specifically, we investigate how the initial conditions with which the electron reaches the continuum influence such an interference, and which consequences this has on the ATI or HHG spectra. We show that the attosecond pulses can be used for controlling this interference, and explain the features observed in [6, 7, 8] in terms of electron orbits.

This paper is organized as follows: In Sec. II, we briefly discuss the SFA for ATI and HHG, with emphasis on the changes introduced by the attosecond-pulse train. Subsequently (Sec. III), we show how several features of both phenomena are affected by it, and provide physical explanations. Finally, in Sec. IV, we give a summary of such results and state the main conclusions of this work.

## II. TRANSITION AMPLITUDES

### A. Above-threshold ionization

For ATI, we will concentrate on the direct electrons, which reach the detector without rescattering with their parent ion. In this case, the ATI transition amplitude reads

$$b_p(t) = i \int_0^t \mathbf{E}(t')dt' d_z(\mathbf{p} + \mathbf{A}(t'))e^{iS(\mathbf{p},t,t')}, \qquad (1)$$

with the action

$$S(p,t,t') = -\int_{t'}^{t} \left( \frac{[p + A(t'')]^2}{2} + I_p \right) dt''. \qquad (2)$$

Eq. (1) can be understood as follows: At an instant $t'$, an electron is ejected by the external laser field from the atomic state in which it is initially bound, reaching a continuum state. It then remains in the continuum until a time $t$, when it reaches the detector with final momentum $\mathbf{p}$. In Eq. (1), $\mathbf{A}(t)$, $I_p$, and $\mathbf{E}(t') = -d\mathbf{A}(t')/dt'$ denote the vector potential, the atomic ionization potential, and the electric field at the time of its release, respectively. We take the dipole matrix element $d_z(\mathbf{p}+\mathbf{A}(t)) = \langle \mathbf{p} + \mathbf{A}(t)| \, \mathbf{r}.\epsilon_z \, |\psi_0\rangle$ for an initial $1s$ state, where the vector $\epsilon_z$ denotes the polarization axis. Specifically, this yields

$$d_z(\mathbf{p}) = i \left( \frac{2^{19/4} I_p^{5/4}}{\pi} \right) \frac{\mathbf{p}.\epsilon_z}{[\mathbf{p}^2 + 2I_p]^3} \qquad (3)$$

We will now write the transition amplitudes for the specific case in which an attosecond-pulse train is present. We assume that this train is composed of an infinite number of odd harmonics. This yields

$$\mathbf{E}_{\rm atto}(t) = E_h \pi \sum_{n=0}^{\infty} \frac{(-1)^n}{\sigma(t)} \delta(t - \frac{n\pi}{\omega})\epsilon_z, \qquad (4)$$

where $\omega$, $E_h$, and $\sigma(t)$ denote the laser field frequency, the attosecond-pulse strength and the train temporal envelope, respectively. In this paper, we assume that the envelope is either given by

$$\sigma(t) \sim \exp[\zeta|t|], \qquad (5)$$

where $\zeta \ll 1$, or by $\sigma = const$. Physically, the latter case corresponds to an infinitely long attosecond-pulse train. We approximate the laser field by a monochromatic wave $\mathbf{E}_l(t) = -d\mathbf{A}_l(t)/dt$, with the vector potential $\mathbf{A}_l(t) = 2\sqrt{U_p}\cos(\omega t - \phi)\epsilon_z$ of frequency $\omega$ dephased of $\phi$ with respect to the attosecond-pulse train.

We now assume that the attosecond pulse train releases the electron in the continuum and that its subsequent propagation is determined only by the monochromatic field. This implies that $\mathbf{E}(t') \simeq \mathbf{E}_{\rm atto}(t')$ and $\mathbf{A}(t) \simeq \mathbf{A}_l(t)$ in Eq. (1). For the direct ATI electrons, such assumptions lead to the transition amplitude

$$\begin{aligned} b_p \;\sim\; & [d_+ \cos\alpha - i d_- \sin\alpha]\chi(a^{(o)}, \zeta\pi/\omega) \\ & + [d_- \cos\alpha - i d_+ \sin\alpha]\chi(a^{(e)}, \zeta\pi/\omega), \end{aligned} \qquad (6)$$

where $d_\pm = d_z(\mathbf{p}+\mathbf{A}(t')) \pm d_z(\mathbf{p}-\mathbf{A}(t'))$, $\theta$ gives the angle between the laser field and the final electron momentum, and the argument $\alpha = 2p\sqrt{U_p}/\omega \cos\theta \sin\phi$ comes from the non-trivial part of the action. Furthermore, in Eq. (6),

$$\chi(a, \zeta\pi/\omega) = \frac{\sinh(\zeta\pi/\omega)}{-\cos(a) + \cosh(\zeta\pi/\omega)}, \qquad (7)$$

$a^{(o)} = (I_p + U_p + p^2/2 - \omega)\pi/\omega$ and $a^{(e)} = (I_p + U_p + p^2/2)\pi/\omega$, respectively. Eq. (7) exhibits sharp peaks at $\cos a = 1$ (i.e., for $a = 2n\pi$). Specifically, $a^{(o)}$ and $a^{(e)}$ lead to expressions with steep maxima around the odd and even ATI peaks, respectively.

In the limit of infinitely long attosecond-pulse trains, $b_p = b_p^{(e)} + b_p^{(o)}$, where

$$b_p^{(e)} \sim \sum_n [d_- \cos\alpha - i d_+ \sin\alpha] \, \delta(\frac{p^2}{2} + U_p + I_p - 2n\omega) \qquad (8)$$

and

$$b_p^{(o)} \sim \sum_n \left[d_+ \cos\alpha - i d_- \sin\alpha\right] \delta(\frac{p^2}{2}+U_p+I_p-(2n+1)\omega), \tag{9}$$

gives the contributions from the even and odd ATI peaks, respectively [20]. In Eq. (8) and (9), one can explicitly notice that the electron leaves with vanishing momentum if $2n\omega = (I_p + U_p)$. Physically, this means that the ionization potential $I_p$ is effectively shifted by the ponderomotive potential $U_p$. Such an effect is noticeable for relatively high driving-field intensities.

In some of the subsequent results, in order to perform a more direct comparison with the results existing in the literature, we will integrate the photoelectron yield over the solid angle. In this case, the yield will be given by

$$\eta(p) = 2\pi \int_{-1}^{1} |b_p|^2 d(\cos\theta), \tag{10}$$

where $b_p$ is given by Eq. (6).

Furthermore, apart from initial 1s states, we will consider the so-called broad gaussian (GBR) approximation, for which $d_z(\mathbf{p} + \mathbf{A}(t)) = const.$ Physically, this approximation means that the electron is initially in an extremely localized bound state (for details see, e.g., [16]). In this particular case, and in the limit of infinitely long attosecond-pulse trains, the integral (10) can be solved analytically and gives

$$\eta(p) \sim 1 \pm \frac{\sin(2\alpha_0)}{2\alpha_0}, \tag{11}$$

where $\alpha_0 = 2p\sqrt{U_p}/\omega \sin\phi$, and the positive and negative signs correspond to the odd and even ATI peaks, respectively.

### B. High-harmonic generation

The HHG transition amplitude is given by an expression which is slightly different from Eq. (1), namely

$$b_\Omega = i \int_{-\infty}^{\infty} dt \int_{-\infty}^{t} dt' \int d^3k d_z^*(\mathbf{k} + \mathbf{A}(t)) d_z(\mathbf{k} + \mathbf{A}(t')) \\ E(t') \exp[iS(t, t', \Omega, \mathbf{k})], \tag{12}$$

with the action

$$S(t, t', \Omega, \mathbf{k}) = -\frac{1}{2} \int_{t'}^{t} [\mathbf{k}+\mathbf{A}(\tau)]^2 d\tau - I_p(t-t') + \Omega t. \tag{13}$$

Eq. 12 describes a physical process in which an electron is freed at a time $t'$, propagates in the continuum with momentum $\mathbf{k}$ from $t'$ to $t$, and, at this time, recombines with its parent ion, generating a harmonic of frequency $\Omega$.

We will now apply the same physical assumptions as in the previous sections to the transition amplitude (12). We will, however, adopt a slightly different convention: instead of considering the time delay in the infra-red field, we will take $\mathbf{A}_l(t) = 2\sqrt{U_p}\cos(\omega t)e_z$ and insert the delay $t_d = \phi/\omega$ in the attosecond pulses. Such a convention will facilitate the discussions in Sec. III.B, in terms of electron orbits. Under such assumptions, Eq. (12) reads

$$b_\Omega = \frac{i\pi E_\mathrm{h}}{\sigma} \sum_{n=0}^{\infty} (-1)^n \int_{-\infty}^{+\infty} dt \int d^3k \exp\left[iS(t, t'_n, \Omega, \mathbf{k})\right] \\ d_z^*(\mathbf{k} + \mathbf{A}_l(t)) d_z(\mathbf{k} + \mathbf{A}_l(t'_n)). \tag{14}$$

In this case, the ionization time is being fixed at $t'_n = t_d + n\pi/\omega$, with $n$ an integer, because the electron is being released into the continuum at such an instant by the attosecond pulses.

The transition amplitude is further simplified in the sense that only the integrals in $\mathbf{k}$ and $t$ must be solved. We evaluate this equation employing saddle-point methods. For that purpose, we consider $\mathbf{k}$ and $t$ so that $S(t, t', \Omega, \mathbf{k})$ is stationary, i.e., that $\partial S/\partial \mathbf{k} = \mathbf{0}$ and $\partial S/\partial t = 0$. This yields the saddle-point equations

$$\int_{t'_n}^{t} d\tau \left[\mathbf{k} + \mathbf{A}_l(\tau)\right] = 0, \tag{15}$$

and

$$2(\Omega - I_p) = \left[\mathbf{k} + \mathbf{A}_l(t)\right]^2, \tag{16}$$

whose solutions can be directly associated to the classical orbits of an electron returning to [Eq. (15)] and recombining with [Eq. (16)] its parent ion [18]. In the presence of the attosecond-pulse train the saddle-point equations for $t$ and $\mathbf{k}$ can be combined, so that the electron return time is given by

$$\sin\omega t - (-1)^n \sin\omega t_d \\ = \left[\omega(t - t_d) - n\pi)\right] \left(\cos\omega t \mp \sqrt{(\Omega - I_p)/(2U_p)}\right). \tag{17}$$

For details on the approximation employed we refer to Ref. [21].

Alternatively, one may follow the procedure in Ref. [16], and compute the Fast Fourier transform for the time-dependent dipole moment in the Strong-Field Approximation. Such an approach involves a single saddle point approximation in the intermediate electron momentum, and two numerical integrations. Hence, it possesses the advantage of taking into account all sets of orbits, and not only the above-mentioned pairs. The procedure adopted in this paper, however, allows a more detailed assessment of quantum-interference effects. For comparison, we provide the time-dependent equations employed in [16], together with a brief discussion, in the appendix.

## III. RESULTS

### A. Above-threshold ionization

As a starting point, we will investigate the effect reported in [8], in which the yield extends to much higher energies for vanishing delay. In [8], this is justified by the following argument: if the electron leaves the atom at the zero of the IR field (i.e., at $\phi = n\pi$), its vector potential is at is maximum, i.e., $A(t') = \pm 2\sqrt{U_p}$. Hence, when the electron reaches the continuum, under these conditions it acquires maximum possible drift momentum. Therefore, it reaches the detector with higher energies. Since this effect only influences how the electron is ejected in the continuum, this should affect both direct and rescattered electrons equally. Therefore, we expect that Eq. (8) and (9), for the direct electrons, exhibit such a behavior.

Fig. 1 displays ATI spectra obtained from Eq. (6), for time delays $0 \leq \phi \leq 2\pi$. In order to perform a direct comparison with the results in [8], we integrate the yield over the solid angle [Eq. (10)]. In the upper part of the figure [Fig. 1.(a)], we consider the same parameters as in [8], while in the lower part [Fig. 1.(b)] we choose a higher intensity for the IR field [22]. In the figure, there exist two distinct behaviors, within two energy regions. For photoelectron energies near the low-energy end of the spectra, the peaks exhibit maximal intensities near $\phi = (2n+1)\pi/2$, i.e., if the electron is released close to the times for which the electric field is maximal. For higher energies, the yield presents a clear minimum around such a delay, and the spectra extends to much higher energy ranges if the delay is vanishing, i.e., if the electron reaches the continuum at the electric-field crossings. This behavior agrees with the findings in [8], and becomes more extreme as the laser-field intensity increases.

Both energy regions appear to be dependent on the driving-field intensity. For instance, for Fig. 1.(a), maxima near $\phi = (2n+1)\pi/2$ are observed roughly for ATI orders $12 \lesssim N \lesssim 20$ ($0 \lesssim p^2/2 \lesssim 13.3eV$), while for Fig. 1.(b), this region lies within $32 \lesssim N \lesssim 40$ ($0 \lesssim p^2/2 \lesssim 16.4eV$). Beyond such energy regions, the yield exhibit minima for such delays. Apart from that, for high-energy photoelectrons, there exist additional minima for the higher driving-field intensity [c.f. Fig. 1.(b)].

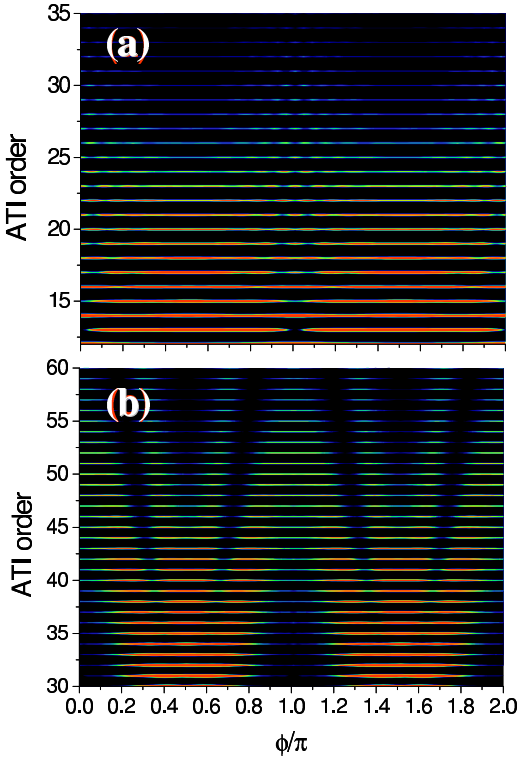


FIG. 1: (Color online) Direct above-threshold ionization spectra, integrated over the solid angle and in linear scale (Eq. (10)), for argon ($I_p = 0.58$ a.u.) interacting with a monochromatic field of frequency $\omega = 0.057$ a.u. and an attosecond-pulse train (Eq. (4)), as functions of the time delay between both driving fields. Panels (a) and (b) have been computed for an intensity of $I = 3.3 \times 10^{13}\mathrm{W/cm^2}$ and $I = 5 \times 10^{14}\mathrm{W/cm^2}$ for the low-frequency laser field, respectively. In panels (a) and (b), the ATI orders (labelled with the number of photons from the ground state) correspond to photoelectron energies roughly between 0 and 36.5 eV, and 0 and 47.4 eV, respectively, due to the ponderomotive shift. The yield has been computed from Eq. (6), with $\zeta = 0.04$. The intensities of the attosecond pulse trains have been chosen as $I_h = I/10$, i.e., one tenth of those of the low-frequency field.

Such a behavior can be readily seen from Eqs. (8) and (9), or, more specifically, from the angle-integrated yield [Eq.(10)]. Indeed, we expect $\eta_p$ to be the superposition of two types of contributions, coming respectively from the non-trivial part of the action $\alpha$ and from the dipole matrix elements $d\pm$. Physically, the former corresponds to the phase the electron acquired leaving at a particular instant, and the latter are specific to the initial state in which the electron is bound.

In Fig. 2, we display the isolated contributions from such terms, integrated over the solid angle [Eq. (10)], for distinct ATI orders. In order to disentangle the effect due to the dipole matrix element and that due to the non-trivial part of the action, in addition to considering 1s initial states, we computed spectra in the broad gaussian (GBR) approximation, for which $d_z(\mathbf{p} + \mathbf{A}(t)) = const$ [Eq. (11)]. In this case, $d_+ = 1$ and $d_- = 0$, so that the effect caused by the non-trivial part of the action, i.e., $\sin\alpha$ and $\cos\alpha$ in Eq. (6), can be directly visualized (c.f. gray curves in the upper panels).

We observe that the non-trivial part of the action leads to a highly oscillating pattern, which, for even or odd ATI peaks, have maxima or minima at $\phi = n\pi$, respectively. As the electron energy increases, the oscillating region becomes increasingly flatter, and the amplitude of the

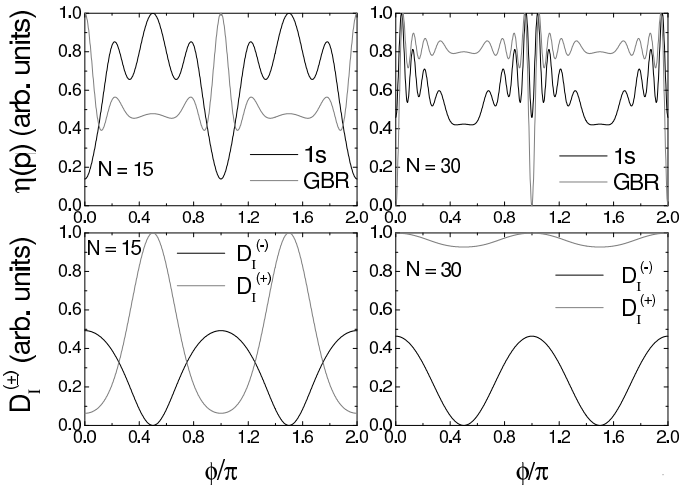


FIG. 2: Upper panels: modulus squared of the transition amplitudes (8) and (9), integrated over the solid angle, for 1s initial states (black line) and within the broad gaussian approximation (grey line), as functions of the time delay between the attosecond-pulse train and the IR field. Lower panels: $|d_+|^2$ and $|d_-|^2$ integrated over the solid angle, for $1s$ initial states. We considered argon under the influence of an IR field of $I = 3.3 \times 10^{13}$W/cm$^2$ superposed to an attosecond-pulse train of $I_h = I/10$ (Panel (a) in Fig. 2). The curves in the upper panels have been normalized so that their maximum values are unity, and those in the lower panel to the maximum value of $D_I^{(-)}$. The numbers N in the figure denote the ATI orders.

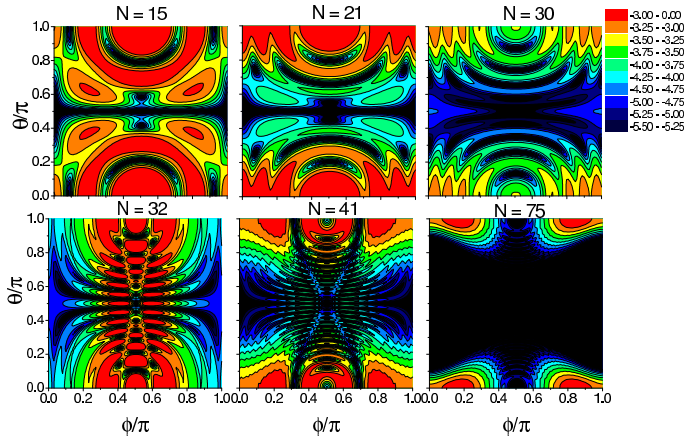


FIG. 3: (Color online) Angular distributions for the ATI direct electrons, in a logarithmic scale, for the same field and atomic parameters as in Fig. 1. The upper and lower panels have been computed for an intensity of $I = 3.3 \times 10^{13}$W/cm$^2$ and $I = 5 \times 10^{14}$W/cm$^2$ for the low-frequency laser field, respectively. The yields are displayed as functions of the time delay $\phi = \omega t_d$ and orientation angle $\theta$ between the laser field and the final electron momenta. The ATI orders N are indicated on the upper parts of the panels, and all contours have been normalized to the highest yield in the figure (left panels).

oscillations are always larger near $\phi = n\pi$. It is, however, clear that the action, by itself, is not responsible for the behavior exhibited in Fig. 1 and shown in detail in Fig. 2, for initial $1s$ states (c.f. black curves in the upper panels). In fact, even though this term leads to several extrema, it does not cause an overall enhancement or suppression of the yield near $\phi = n\pi$, as observed for the low- and high-order ATI peaks respectively.

The integral

$$D_I^{(\pm)} = 2\pi \int_{-1}^{1} |d_\pm|^2 d(cos\theta) \qquad (18)$$

of $|d_\pm|^2$ over the solid angle sheds some light in this behavior (c.f. lower panels in Fig. 2). The contributions from $d_-$ exhibit a minimum at $\phi = (2n+1)\pi/2$, while the behavior of those from $d_+$ depend on the energy region in question. Near the ionization threshold, the latter contributions exhibit maxima near the delays $\phi = (2n+1)\pi/2$. As the ATI order increases, such maxima become flatter, until the concavity of $D_I^{(+)}$ changes and the yield starts to exhibit maxima at $\phi = n\pi$. Such contributions are dominant, with respect to those from $d_-$, and are present both in Eq. (8) and (9). This behavior gets more pronounced as the driving-field intensity increases (higher intensities lead also to sets of secondary maxima in $D_I^{(\pm)}$, which contribute to the additional structure observed in Fig. 1.(b)). One should also note that, very near the threshold, for $\phi = n\pi$, $D_I^{(-)} > D_I^{(+)}$. This causes the minima observed for $\eta(p)$ in Fig. 1(a), for initial $1s$ states. In contrast, the yield from the broad-gaussian approximation exhibits maxima in this case.

Therefore, the behavior reported in [8] is not only due to the phase the electron obtains when it is ejected in the continuum by the attosecond-pulse train, or, in other words, to the momentum transfer from the field to the electron. Additionally, it is related to the initial state in which the electron is bound, which, in our model, is a $1s$ state. Indeed, such a behavior is absent in the broad gaussian approximation, which, physically, corresponds to an electron initially bound in a highly localized state. Such a strong dependence on the initial electronic bound state is, in a sense, quite unusual for phenomena occurring in the context of atoms in strong laser fields.

The ATI angular distributions, depicted in Fig. 3, confirm this trend. In fact, the figure shows distributions symmetric upon $\theta \to \pi - \theta$ and $\phi \to \pi - \phi$, in which it is possible to identify three distinct energy regions. Near the threshold ($N = 15$ and $N = 32$ for the lower and higher intensity, respectively), there exist annular maxima, centered around $\phi = \pi/2$. Such maxima are most pronounced for $\theta = 0$ and $\theta = \pi$, but also occur for other alignment angles. As the photoelectron energy increases (middle and right panels in the figure), the ring-shaped maxima split and move towards $\phi = n\pi$ and $\theta = n\pi$, which are the maxima observed for high enough ATI or-

ders. Other, less pronounced maxima are also seen, as well as additional substructure. Such a pattern is due to interference effects and comes from the non-trivial part of the action. As the driving-field intensity increases, this pattern gets more complicated, but the overall behavior remains.

### B. High-harmonic generation

Subsequently, we address the question of whether the effects reported in [6, 7], for HHG in a near-infrared laser field superposed to a time-delayed attosecond-pulse train, are present in our framework. Specifically, intensity variations from one to two orders of magnitude in the plateau harmonics have been observed, whose prominence, and even existence, was strongly affected by the time delay $\phi = \omega t_d$. Moreover, the resolution of the harmonic peaks, and the plateau structure, with enhancements of either *all* plateau harmonics, or only near its low-energy end, were observed to depend very much on this parameter.

In [6], such effects have been attributed to quantum-trajectory selection: In HHG, in the absence of the attosecond pulses, there exists one set of trajectories, which mainly contribute to the yield. Such trajectories merge at the cutoff, i.e., the maximal energy for which HHG occurs, and correspond to a longer and a shorter excursion time for the electron in the continuum [12]. By using an attosecond-pulse train, one is splitting this set into two, due to the fact that the electron is released in the continuum with non-vanishing velocity, and, at the same time, selecting a trajectory of this set, by fixing the electron emission time.

Thus, the attosecond pulses allow one to perform quantum-trajectory selection at the single-atom response level. For solely an IR laser field, it is only possible to perform such a selection at the macroscopic level, by controlling the propagation conditions [12]. In support of this argument, classical simulations have been performed in [6] for an electron returning to its parent ion. Thereby, the initial electron velocity has been estimated from the average frequency in the attosecond-pulse train, which in [6], has been composed by five harmonics ($N = 11$ to $N = 19$).

In Fig. 4, we present HHG spectra computed with Eq. (14), in the broad gaussian approximation. Such spectra are highly dependent on the time delay $t_d$ between the low-frequency field and the attosecond-pulse train, and differ in the cutoff energy, and in the high-harmonic strengths and resolutions. Specifically, in the examples provided in the figure, the cutoff energies vary from roughly $I_p + 1.8U_p$ [Fig. 4.(a)] to $I_p + 2.5U_p$ [Fig. 4.(c)], and the intensities of the plateau harmonics differ in up to two orders of magnitude. Furthermore, for particular time delays, the plateau harmonics are unequally enhanced. For instance, in Figs. 4.(b) and 4.(c), the low-plateau harmonics are more than one order of magnitude larger than those near its high-energy end. Such a group

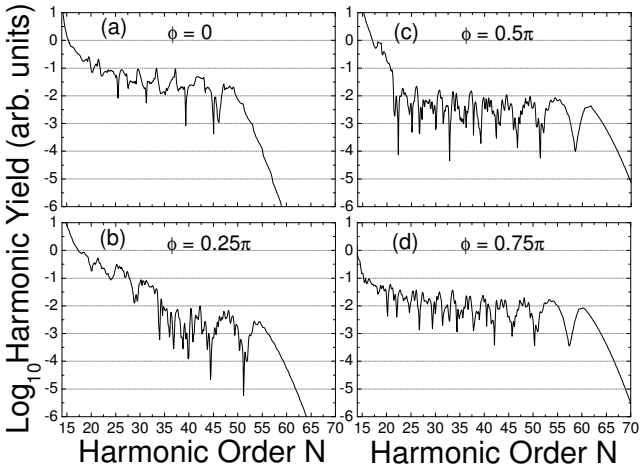


FIG. 4: High-harmonic spectra for neon ($I_p = 0.79$ a.u.) interacting with a monochromatic field of intensity $I = 5 \times 10^{14}\mathrm{W/cm^2}$, and frequency $\omega = 0.057$ a.u., and a train of attosecond pulses of intensity $I_\mathrm{h} = 10^{13}\mathrm{W/cm^2}$ (Eq. (4)), and several time delays between the attosecond pulse train and the IR field. We considered the orbits with the five shortest pairs of excursion times $t - t'$. In the figure, we only show the harmonic orders for which $\Omega > I_p$.

varies from the lower half [Fig. 4.(b)] to the lowest few harmonics [Fig. 4.(c)] of the plateau. The spectra are identical over $\omega t_d \to \omega t_d \pm \pi$ (not shown). This is a consequence of the fact that $|d_\Omega(\omega t_d)|^2 = |d_\Omega(\omega t_d \pm \pi)|^2$. In particular, for $\omega t_d = n\pi$, the plateau harmonics exhibit maximal intensities in this context.

The effects observed in Fig. 4 are in qualitative agreement with those reported in [6, 7]. In order to find out whether they are due to quantum-orbit selection, they will be analyzed in terms of the orbits of an electron recombining with its parent ion. For that purpose, we solve Eq. (17) for a fixed start time. The real parts of its solutions can be directly associated to the return times $t$ of a classical electron in an external field.

Fig. 5 depicts the real parts of such return times for the six shortest orbits, as functions of the harmonic order, for the time delays in the previous figure. The orbits are denoted by the numbers $(i, j)$, which increase with the electron excursion time in the continuum. Depending on the time delay, the return times, and the maximal harmonic energies are significantly altered. This shows that the changes in the initial conditions of the electron being ejected considerably affect its subsequent dynamics. Furthermore, the return times occur in pairs, i.e., for a single ionization time, there is always a shorter and a longer travel time for the electron in the continuum. Such pairs of orbits coalesce at the maximally allowed harmonic energies, which considerably vary with the delay $\phi$. Such variations are explicitly given in Table I. In particular,

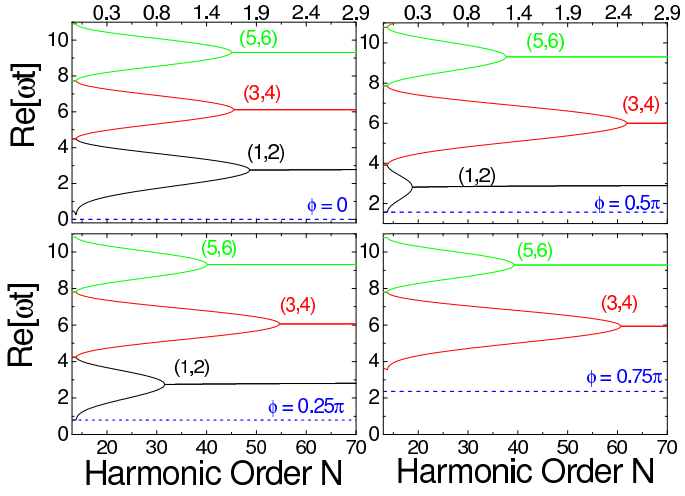


FIG. 5: (Color online) Real part of the recombination times as a function of the high-harmonic order, for neon ($I_p = 0.79$ a.u.) interacting with a monochromatic field of intensity $I = 5 \times 10^{14}$W/cm$^2$, and frequency $\omega = 0.057$ a.u. and an attosecond-pulse train of intensity $I_h = 10^{13}$W/cm$^2$, composed of an infinite number of harmonics (Eq. (4)). Parts (a), (b), (c) and (d) correspond to delays $\phi = 0$, $\phi = 0.25\pi$, $\phi = 0.5\pi$ and $\phi = 0.75\pi$ between the attosecond-pulse train and the low-frequency driving wave, respectively. In the figure, we only show the harmonic orders for which $\Omega > I_p$, and the pairs of orbits are indicated by the natural numbers $(i, j)$, which increase according to the electron excursion time in the continuum. The ionization times are indicated by the blue dashed lines, and the numbers in the upper part of the figure give the approximate kinetic energy of the electron upon return, in units of the ponderomotive energy $U_p$.

| Orbits | $E_{\rm kin}(t,t')/U_p$ | | | |
|---|---|---|---|---|
| | $\phi = 0$ | $\phi = 0.25\pi$ | $\phi = 0..5\pi$ | $\phi = 0.75\pi$ |
| (1,2) | 1.80 | 0.93 | 0.26 | – |
| (3,4) | 1.65 | 2.11 | 2.50 | 2.43 |
| (5,6) | 1.62 | 1.37 | 1.25 | 1.32 |

TABLE I: Maximum kinetic energies $E_{\rm kin}(t,t') = (N\omega - I_p)/U_p$, in units of the ponderomotive energy, for an electron along the three pairs of orbits displayed in Fig. 5. No entry means that this energy is very close to the ionization potential.

the largest variations occur for the set of orbits (1,2), namely from the ionization potential to $I_p + 1.8U_p$.

Each of such local maxima potentially corresponds to a cutoff in the harmonic spectra. Whether, however, they will lead to only minor features or to a sharp decrease in the high-harmonic yield will depend on three main issues. First, it is necessary that the electron reaches the continuum with a large ionization probability. Second, due to the fact that the electronic wave packet spreads with time, it is desirable that such a wave packet spends as little time as possible in the continuum. This yields a large overlap between such a wave packet and that of a bound electron, and, consequently, prominent harmonics. Finally, there may be effects related to quantum interference, which suppress or enhance particular sets of harmonics. Since, due to the attosecond-pulse train, the electron is being ejected with a large probability for all cases, we expect that the main difference will be due to wave-packet spreading. Hence, the shorter the electron excursion time $\tau = t - t'$ in the continuum is, the more prominent the corresponding harmonics should be.

We will now analyze the contributions of each pair of orbits to the spectrum. Such contributions are presented in Fig. 6. Panel 6.(a) shows that, for an attosecond-pulse train in phase with the low-frequency field, the main contributions come from the orbits $(1, 2)$. This occurs for two main reasons. First, the harmonics from this set of orbits are two orders of magnitude larger than those from the remaining pairs. This is a consequence of the fact that $\tau$ is very short for such a pair. Furthermore, for this specific phase, the cutoff energy for $(1, 2)$ extends to a relatively large harmonic order (c.f. Fig. 5 and Table 1), so that the contributions from the remaining pairs of orbits are overshadowed.

For a delay of $\phi = 0.25\pi$ [Fig. 6.(b)], this picture starts to change. In fact, although the harmonics from (1,2) are much stronger than those from the remaining pairs, the maximal kinetic energy for $(1, 2)$ lies near a much lower harmonic order (near $N = 35$). Thus, beyond such energy, the corresponding contributions are exponentially decaying and the harmonics intensities, as well as the cutoff energy near $2.11U_p$, are mainly determined by $(3, 4)$. This causes the double plateau structure in the figure, and provides an alternative explanation for the enhancements only in the low-plateau harmonics reported in [6].

For $\phi = 0.5\pi$ [Fig. 6.(c)], instead, there is a very steep intensity drop at the the low-energy end of the plateau. This is a consequence of the very low cutoff for the orbits $(1, 2)$, near the $19^{\rm th}$ harmonic. For higher energies, the main behavior in the spectrum is determined by $(3, 4)$. Finally, for $\phi = 0.75\pi$ [Fig. 6.(d)], the maximal energy for $(1, 2)$ is so close to the ionization potential, that such a pair does not play any role. Consequently, there is an overall decrease of at least one order of magnitude in the spectrum. At the same time, the orbits (3,4) become increasingly shorter. Around $\omega t_d = 0.75\pi$, such latter orbits have become the shortest contributing and the intensity starts to increase, until, at $\omega t_d = \pi$, the same pattern as for vanishing time delay is recovered. The contributions from pairs of orbits with longer excursion times are much less relevant due to wave-packet spreading.

Structured spectra, however, are only obtained if several pairs of orbits are taken into account. One should note that, if one employs orbits starting from (3,4) and vanishing time delays between the attosecond-pulse train and the IR field, there seems to be an improvement in the resolution of the spectra (c.f. blue line in Fig. 6.(a)).

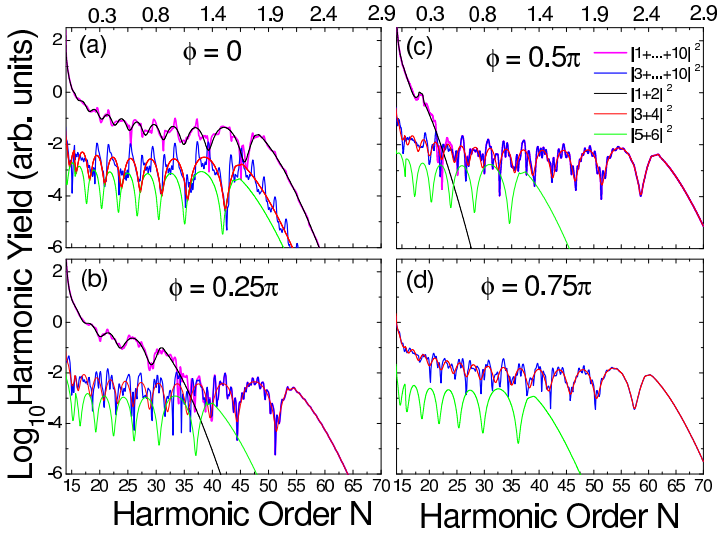


FIG. 6: (Color online) Contributions of isolated pairs of orbits to the high-harmonic spectra for the same atomic and external-field parameters in Figs. 4 and 5, and delays $\phi = 0$, $\phi = 0.25\pi$, $\phi = 0.5\pi$ and $\phi = 0.75\pi$ between the attosecond-pulse train and the low-frequency driving wave (Figs. 6(a), 6.(b), 6.(c) and 6.(d), respectively). In the figure, we only show the harmonic orders for which $\Omega > I_p$. The contributions from specific pairs of orbits are depicted in the same colors as those employed in Fig. 5, for depicting each corresponding pair. For comparison, the spectra computed with the ten shortest orbits and with orbit 3 to 10 are given as the thick lines in the figure. The numbers on the upper parts of the figure give the approximate kinetic energy of the electron upon return, in units of the ponderomotive energy.

In [6], resolved harmonics have been related to selecting a particular trajectory for the returning electron. In our case, however, it appears to be an interference effect between several orbits for the returning electron. The fast oscillations observed here are possibly not harmonics (due to the periodicity of the process), but are caused by the interference of different quantum orbits originating from (launched from) the same half cycle.

With regard to the above discussion, we should point out that the absence of discrete harmonics in the spectra displayed in this work is due to the fact that we are considering orbits starting only in the first cycle of the laser field, instead of over many cycles. Therefore, we do not have enough periodicity to obtain discrete harmonic peaks. This is however not a problem in our context, since we concentrate our investigations on how quantum-interference effects influence the main structure of the spectra. By considering a restricted range of electron start times, such effects can be more clearly seen and interpreted.

The above-discussed behavior is very similar to that observed in [6]. Figs. 4-6, however, have been plotted for a set of time delays different from those employed in such a reference. Such discrepancies may be related to the fact that, in [6], only a finite and relatively small group of harmonics has been used, whereas, in our computations, we have employed the attosecond-pulse limit for an infinite set of harmonics.

In fact, if the attosecond-pulse train is composed by a relatively small number of harmonics (such as in [6]), it is possible to define a main frequency for this train. Hence, it is reasonable to assume that electron is being ejected in the continuum by a photon of such a frequency, and thus with nonvanishing velocity. This will cause a splitting of the trajectories into the "downhill" and "uphill" transitions, which correspond to the ejection of the electron in- or opposite to- the direction of the laser field, respectively, and which will be selected according to the time delay.

On the other hand, if the attosecond pulse train is composed by an infinite number of frequencies, the uncertainty relation will no longer allow one to define a main frequency for it. Consequently, the physical picture of an electron being released by a photon of a specific frequency and reaching the continuum with a constant velocity is no longer applicable. However, it is still possible to define a specific time $t'$ for which the electron is ejected, and determine the corresponding return times.

## IV. CONCLUSIONS

In conclusion, we have shown that an attosecond-pulse train superposed to a strong, near-infrared laser field can be used for controlling above-threshold ionization (ATI) and high-order harmonic generation (HHG). This control is exerted by using the attosecond pulses, which are time delayed with respect to the infrared field, to constrain the instant in which an electronic wave packet is ejected in the continuum. Since this wave packet will either recombine with its parent ion, generating high harmonics, or contribute to the above-threshold ionization spectrum, both phenomena are strongly affected by such pulses.

Similar investigations, which led to similar effects to those in this paper, have been performed in [6, 8], employing the numerical solution of the Schrödinger equation. In this work, however, we go beyond such studies, and trace all features observed to quantum-interference effects between the possible pathways of the electronic wave packet. In particular, the model used in this paper, based on the Strong-Field Approximation (SFA) allows one to investigate the different ingredients involved in the computation of the transition amplitude, and how they are influenced by the attosecond-pulse train, in a detailed and transparent way.

For ATI, we restrict ourselves to the direct electrons, i.e., those that reach the detector without rescattering with its parent ion. We consider an attosecond-pulse train composed by an infinite group of harmonics and we sum over all periods of the driving field. In this case, we observed an extension in the photoelectron energy if the attosecond-pulse train is in phase with the IR field (i.e.,

for delays $\phi = n\pi$).

In [8], this has been attributed to the fact that, in this case, the electrons are ejected at a zero crossing of the IR field. Hence, they gain the maximal possible momentum from the field, namely $p = \pm 2\sqrt{U_p}$. In this paper, we have shown that this mechanism does play a role, which, in our framework, is implicit in the non-trivial part of the action. However, in order to obtain the above-mentioned effect, the dipole matrix elements from a 1s hydrogenic state are also a necessary ingredient. Physically, such matrix elements are related to the initial state where the electron is bound and, in the SFA, contain all the information about the atomic bound potential. Furthermore, we have shown that such an effect only occurs if the photoelectron energy is sufficiently far from the ionization threshold. In fact, for low ATI orders, maximal intensities are obtained for $\phi = (2n+1)\pi/2$. This is also due to an interplay between the phase the electron acquires when it reaches the continuum and its initial bound state.

Apart from such studies, we have observed that the ATI angular distributions are strongly dependent on this delay, and on the photoelectron energy. Near the ionization threshold, such distributions exhibit very pronounced maxima for backscattered electrons (alignment angle $\theta = n\pi$) which leave at peak-field times ($\phi = (2n+1)\pi/2$). As the photoelectron energies increase, such maxima move towards the zero crossings of the electric field ($\phi = 2n\pi$). This behavior is in agreement with that observed for the ATI spectra.

For HHG, depending on the time delay between the attosecond-pulse train and the IR field, we observed deviations in almost 30% in the cutoff energy. Furthermore, the plateau structure is highly sensitive to the time delay $\phi$. Indeed, we found that, for certain ranges of this parameter, the low-plateau harmonics are one to two orders of magnitude stronger than those near its high-energy end. The precise sets of harmonics in such a double-plateau structure depend very much on $\phi$. For our particular parameters, the set of strong harmonics moved towards lower energies as $\phi$ distanced itself from a zero crossing of the electric field.

Our results can be traced back to the interplay of two sets of orbits for an electron returning to its parent ion. Specifically, the maximal return electron energy in the shortest set of orbits changes from 0 to $1.8U_p$, as the ejection time of the electron is varied. These orbits yield a group of very strong harmonics, whose extension can be manipulated by controlling the time delay $\phi$. The remaining harmonics are mainly determined by the second shortest pair of orbits, and are considerably weaker.

In this context, a noteworthy aspect is that, in contrast to ATI, for which the effects mentioned in this paper also depend on the initial electron state, in HHG they appear to be due to controlling electron orbits with an attosecond-pulse train. Indeed, whereas in ATI such effects do not occur for initial localized bound states, i.e., in the broad gaussian approximation, for HHG they are already present in this case.

The results for HHG also agree to a great extent with those reported in [6]. However, their interpretation, as well as the time delays for which they occur, are somewhat different. In fact, in [6], all features are explained by selecting a single orbit from the shortest pair, and by the splitting in this set of orbits due to the fact that the electron is reaching the continuum with non-vanishing velocity. Such differences are possibly due to the fact that, in [6], only a small group of harmonics has been employed for producing the attosecond-pulse train, while, in Eq. (4), we consider the limit of an infinite number of harmonics. We therefore expect the agreement to increase if a larger number of harmonics is taken when constructing the attosecond-pulse-train.

## V. APPENDIX

In this appendix, we explicitly provide the time-dependent expression adopted in Ref. [16]. In this case, the time-dependent dipole moment reads

$$d(t) = i\int_{-\infty}^{t} dt' \int d^3k d_z^*(\mathbf{k}+\mathbf{A}(t)) d_z(\mathbf{k}+\mathbf{A}(t')) E(t') \exp[iS(t,t',\mathbf{k})], \quad (19)$$

with the action

$$S(t,t',\mathbf{k}) = -\frac{1}{2}\int_{t'}^{t} [\mathbf{k}+\mathbf{A}(\tau)]^2 d\tau - I_p(t-t'). \quad (20)$$

Alternatively to the procedure adopted in this paper, one may integrate Eq.(19) over the intermediate momentum using the saddle point equation (15). This yields the equation

$$b_t = \frac{i\pi E_h}{\sigma}\sum_{n=0}^{\infty}(-1)^n \int_{-\infty}^{t} (2\pi/i(t-t'_n+i\epsilon))^{3/2} d_z^*(\mathbf{k}_{st}+\mathbf{A}(t)) d_z(\mathbf{k}_{st}+\mathbf{A}(t'_n)) \exp[iS(t,t'_n,\mathbf{k}_{st})], \quad (21)$$

with the action given by formula (20), to which a Fast Fourier transform routine is then applied. In Eq. (21), $\mathbf{k}_{st} = -(1/(t-t'_n))\int_{t'_n}^{t} d\tau \mathbf{A}(\tau)$, and the sum extends over $t'_n \leq t$. Due to the wave-packet-spreading effects (described by the $((2\pi/i(t-t'_n+i\epsilon))^{3/2}$), the main contributions to the sum in Eq. (21) come from few $t'_n$ that are the closest to $t$.

### Acknowledgments

This work has been financed in part by the Deutsche Forschungsgemeinschaft (European Graduate College "Interference and Quantum Applications", SFB407, SPP1078 and SPP1116, 436POL)), spanish MEC grant FIS-2005-04627, the ESF Program QUDEDIS, and the Marie Curie European Program MRTN-CT-2003-505138,XTRA. C.F.M.F. would like to thank the ICFO

and the Universidade do Algarve for their kind hospitality.


[1] For a review c.f. P. Agostini and L. DiMauro, Rep. Prog. Phys. **67**, 813 (2004).

[2] M. Hentschel, R. Kienberger, Ch. Spielmann, G.A. Reider, N. Milošević, T. Brabec, P.B. Corkum, U. Heinzmann, M. Drescher and F. Krausz, Nature **414**, 509 (2001).

[3] M. Schnürer, Ch. Streli, P. Wobrauschek, M. Hentschel, R. Kienberger, Ch. Spielmann, and F. Krausz, Phys. Rev. Lett. **85**, 3392 (2000); M. Drescher, M. Hentschel, R. Kienberger, M. Uiberacker, V. Yakovlev, A. Scrinzi, T. Westerwahlbesloh, U. Kleineberg, U. Heinzmann, and F. Krausz, Nature **419**, 803 (2002).

[4] H. Niikura, F. Légaré, R. Hasbani, A. D. Bandrauk, M. Yu. Ivanov, D. M. Villeneuve and P. B. Corkum, Nature **417**, 917 (2002).

[5] R. Kienberger, M. Hentschel, M. Uiberacker, Ch. Spielmann, M. Kitzler, A. Scrinzi, M. Wieland, Th. Westerwalbesloh, U. Kleineberg, U. Heinzmann, M. Drescher, F. Krausz, Science **297**, 1144 (2002); A. Baltuska, Th. Udem, M. Uiberacker, M. Hentschel, E. Goulielmakis, Ch. Gohle, R. Holzwarth, V. S. Yakovlev, A. Scrinzi, T. W. Hänsch, and F. Krausz, Nature **421**, 611 (2003).

[6] K. J. Schafer, M. B. Gaarde, A. Heinrich, J. Biegert, and U. Keller, Phys. Rev. Lett. **92**, 023003 (2004); M. B. Gaarde, K. J. Schafer, A. Heinrich, J. Biegert, and U. Keller, Phys. Rev. A **72**, 013411 (2005); J. Biegert, A. Heinrich, C. P. Hauri, W. Kornelis, P. Schlup, M. P. Anscombe, M. B. Gaarde, K. J. Schafer and U. Keller, J. Mod. Opt. **53**, 87 (2006); J. Biegert, A. Heinrich, C. P. Hauri, W. Kornelis, P. Schlup, M. P. Anscombe, K. J. Schafer, M. B. Gaarde and U. Keller, Laser Physics **15**, 899 (2005).

[7] P. Johnsson, K. Varjú, T. Remetter, E. Gustafsson, J. Mauritsson, R. Lopez-Martens, S. Kazamias, C. Valentin, Ph. Balcou, M. B. Gaarde, K. J. Schafer, and A. L'Huillier, J. Mod. Opt. **53**, 233 (2006).

[8] P. Johnsson, R. López-Martens, S. Kazamias, J. Mauritsson, C. Valentin, T. Remetter, K. Varjú, M. B. Gaarde, Y. Mairesse, H. Wabnitz, P. Salières, Ph. Balcou, K. J. Schafer, and A. L'Huillier, Phys. Rev. Lett. **95**, 013001 (2005).

[9] For a review c.f. T. Brabec and F. Krausz, Rev. Mod. Phys. **72**, 545 (2000).

[10] M. Drescher, M. Hentschel, R. Kienberger, G. Tempea, C. Spielmann, G. A. Reider, P. B. Corkum and F. Krausz, Science **291**, 1923 (2001).

[11] N. A. Papadogianis, B. Witzel, C. Kalpouzos and D. Charalambidis, Phys. Rev. Lett. **83**, 4289 (1999); P. M. Paul, E. S. Toma, P. Breger, G. Mullot, F. Augé, Ph. Balcou, H. G. Muller, and P. Agostini, Science **292**, 1689 (2001).

[12] Ph. Antoine, A. L'Huillier and M. Lewenstein, Phys. Rev. Lett. **77**, 1234 (1996).

[13] Y. Mairesse, A. de Bohan, L. J. Frasinski, H. Merdji, L. C. Dinu, P. Monchicourt, P. Breger, M. Kovačev, R. Taïeb, B. Carré, H. G. Muller, P. Agostini and P. Salières, Science **302**, 1540 (2003).

[14] Y. Mairesse, A. de Bohan, L. J. Frasinski, H. Merdji, L. C. Dinu, P. Monchicourt, P. Breger, M. Kovačev, T. Auguste, B. Carré, H. G. Muller, P. Agostini and P. Salières, Phys. Rev. Lett. **93**, 163901 (2004); J. Mauritsson, P.Johnsson, R. López-Martens, K. Varjú, W. Kornelis, J. Biegert, U. Keller, M. B. Gaarde, K. J. Schafer, and A. L'Huillier, Phys. Rev. A **70**, 021801(R) (2004).

[15] P. B. Corkum, Phys. Rev. Lett. **71**, 1994 (1993); K. C. Kulander, K. J. Schafer, and J. L. Krause in: B. Piraux et al. eds., *Proceedings of the SILAP conference*, (Plenum, New York, 1993).

[16] M. Lewenstein, Ph. Balcou, M. Yu. Ivanov, A. L'Huillier and P. B. Corkum, Phys. Rev. A **49**, 2117 (1994).

[17] W. Becker, S. Long, and J. K. McIver, Phys. Rev. A **41**, 4112 (1990); ibid. **50**, 1540 (1994); M. Lewenstein, K. C. Kulander, K. J. Schafer and Ph. Bucksbaum, Phys. Rev. A **51**, 1495 (1995).

[18] P. Salières, B. Carré, L. LeDéroff, F. Grasbon, G. G. Paulus, H. Walther, R. Kopold, W. Becker, D.B. Milošević, A. Sanpera and M. Lewenstein, Science **292**, 902 (2001).

[19] The SFA consists in neglecting the atomic potential in the propagation of the electron in the continuum, the laser field when the electron is bound or rescatters, and the excited states of the atom in question.

[20] For the parameter range employed in this paper, we obtained practically identical results from such a limit, and from Eq. (6), for $\zeta \lesssim 0.04$.

[21] C. Figueira de Morisson Faria, H. Schomerus and W. Becker, Phys. Rev. A **66**, 043413 (2002).

[22] For this latter intensity, tunneling ionization may also play a role and compete with the ionization induced by the attosecond pulse train. Hence, it may be necessary to take into account tunneling ionization in the transition amplitude (1). This case is, however, considered to illustrate the effects that may arise at high laser intensity.